tvst

Retina

Histologic Cell Shape Descriptors for the Retinal Pigment Epithelium in Age-Related Macular Degeneration: A Comparison to Unaffected Eyes

Leon von der Emde[1], Marc Vaisband[2,3], Jan Hasenauer[2,4], Leonie Bourauel[1], Katharina Bermond[5], Marlene Saßmannshausen[1], Rainer Heintzmann[6,7], Frank G. Holz[1], Christine A. Curcio[8], Kenneth R. Sloan[8], and Thomas Ach[1]

[1] Department of Ophthalmology, University Hospital Bonn, Bonn, Germany
[2] University of Bonn, Life & Medical Sciences Institute, Bonn, Germany
[3] Department of Internal Medicine III with Haematology, Medical Oncology, Haemostaseology, Infectiology and Rheumatology, Oncologic Center; Salzburg Cancer Research Institute–Laboratory for Immunological and Molecular Cancer Research (SCRI-LIMCR); Paracelsus Medical University, Salzburg, Austria, Cancer Cluster Salzburg, Austria
[4] Helmholtz Center Munich- German Research Center for Environmental Health, Institute of Computational Biology, Neuherberg, Germany
[5] Department of Ophthalmology, Ludwigshafen Hospital, Ludwigshafen, Germany
[6] Leibniz Institute of Photonic Technology, Jena, Germany
[7] Institute of Physical Chemistry and Abbe Center of Photonics, Friedrich-Schiller University Jena, Jena, Germany
[8] Department of Ophthalmology and Visual Sciences, University of Alabama at Birmingham, AL, USA

Correspondence: Thomas Ach, Department of Ophthalmology, University of Bonn, Ernst-Abbe-Straße 2, Bonn 53127, Germany.
e-mail: thomas.ach@ukbonn.de

Received: March 28, 2022
Accepted: July 16, 2022
Published: August 19, 2022

Keywords: confocal fluorescence microscopy; shape descriptors; principal component analysis

Citation: von der Emde L, Vaisband M, Hasenauer J, Bourauel L, Bermond K, Saßmannshausen M, Heintzmann R, Holz FG, Curcio CA, Sloan KR, Ach T. Histologic cell shape descriptors for the retinal pigment epithelium in age-related macular degeneration: A comparison to unaffected eyes. Transl Vis Sci Technol. 2022;11(8):19, https://doi.org/10.1167/tvst.11.8.19

Purpose: Phenotype alterations of the retinal pigment epithelium (RPE) are a main characteristic of age-related macular degeneration (AMD). Individual RPE cell shape descriptors may help to delineate healthy from AMD-affected cells in early disease stages.

Methods: Twenty-two human RPE flatmounts (7 eyes with AMD [early, 3; geographic atrophy, 1; neovascular, 3); 15 unaffected eyes [8 aged $\leq$51 years; 7 aged $>$80 years)] were imaged at the fovea, perifovea, and near periphery (predefined sample locations) using a laser-scanning confocal fluorescence microscope. RPE cell boundaries were manually marked with computer assistance. For each cell, 11 shape descriptors were calculated and correlated with donor age, cell autofluorescence (AF) intensity, and retinal location. Statistical analysis was performed using an ensemble classifier based on logistic regression.

Results: In AMD, RPE was altered at all locations (most pronounced at the fovea), with area, solidity, and form factor being the most discriminatory descriptors. In the unaffected macula, aging had no significant effect on cell shape factors; however, with increasing distance to the fovea, area, solidity, and convexity increased while form factor decreased. Reduced AF in AMD was significantly associated with decreased roundness and solidity.

Conclusions: AMD results in an altered RPE with enlarged and deformed cells that could precede clinically visible lesions and thus serve as early biomarkers for AMD onset. Our data may also help guide the interpretation of RPE morphology in in vivo studies utilizing high-resolution single-cell imaging.

Translational Relevance: Our histologic RPE cell shape data have the ability to identify robust biomarkers for the early detection of AMD-affected cells, which also could serve as a basis for automated segmentation of RPE sheets.

Introduction

The retinal pigment epithelium (RPE) is an epithelium of postmitotic cells between Bruch's membrane and the choroid basally and the photoreceptors apically. This monolayer is essential for the health and function of the outer retina. The RPE layer is a sheet of polygonal (mostly hexagonal) cells that is highly adapted to its local requirements in the outer retina, especially to the metabolism, phototransduction, and image sampling demands of the photoreceptors.[1,2]

RPE cell shape is dependent on retinal location, age, and disease. Throughout the posterior pole, there are important spatial differences in the photoreceptor distribution as well as RPE densities and RPE morphology.[3] The healthy cone-only foveola exhibits the highest density of RPE cells, which are also predominantly hexagonal, uniform in size, and strictly mononuclear. Outside the fovea, RPE cells are larger, asymmetrical in shape, and more frequently multinucleate.[4] In aging, RPE cell density in the macula remains constant, but the layer exhibits a more variable number of neighboring cells. In age-related macular degeneration (AMD), RPE cells have been described as irregular and enlarged with the onset of disease.[5] These local variations make systematic sampling a prerequisite for any microscopic study of RPE cells.

Clinically visible autofluorescence (AF) properties of RPE cells rely on the intracellular presence of melanosomes, lipofuscin, and melanolipofuscin granules. Each healthy RPE cell hosts hundreds of lipofuscin and melanolipofuscin granules that exhibit autofluorescence when excited with blue light.[6] Granule distribution varies with retinal location, with a higher number of melanolipofuscin granules in foveal RPE cells than elsewhere. Granule accumulation starts in childhood and continues throughout aging, which, in parallel, results in an increasing fundus AF signal during the life span.[7] At higher age and in AMD, lipofuscin abundance decreases, as seen in histology and manifesting as decreased AF levels in quantitative fundus autofluorescence (QAF) in clinical in vivo imaging.[8–10]

A detailed quantification of cell shape could help to detect AMD-affected RPE cells early on. Currently, Voronoi partitions are commonly used to determine cell shape in an epithelial sheet.[11] While the resulting Voronoi diagrams may be helpful to estimate parameters such as cell number and number of neighboring cells, information regarding shape is lost since Voronoi diagrams do not necessarily represent actual cell shape and boundaries. The use of Voronoi analysis has three key disadvantages in delineating AMD RPE cells. First, Voronoi diagrams assume a convex shape, which disregards irregular cell shapes and spurs that may develop with AMD. Second, statistics derived from Voronoi diagrams require many contiguous cells for validity and thus may not be suitable for specimens with AMD-typical cell loss and anterior migration of RPE cells. Last, autofluorescent granules are absent basolaterally at the RPE cell border, resulting in a hypoautofluorescent gap between cells in en face AF imaging. Voronoi connecting lines between two vertices do not acknowledge this specific granule distribution within RPE cells, which could lead to imprecise cell AF measurements (e.g., hypofluorescent gaps included within the RPE cell), especially in RPE cells with an odd shape, as in AMD.

An alternative to Voronoi diagrams are cell shape descriptors such as roundness, compactness, eccentricity, and form factor of cells. Cell shape descriptors have been broadly used in biology to characterize and differentiate cells or lesions, and it was, for instance, shown that (1) myocyte shape correlates with heart function, and (2) capillary endothelial cell shape governs proliferation, cell growth, and apoptosis.[12–15] In ophthalmology, cell shape descriptors were able to accurately estimate lesion progression rates in geographic atrophy lesions.[12] Applied to RPE cells, shape descriptors could first serve to capture the unique morphology of the RPE in both health and AMD. This knowledge could then support clinical diagnostics, as these cell alterations would be visible early on without the requirement of large affected areas to be visualized. Since RPE cells are now trackable in vivo using adaptive optics scanning laser ophthalmoscopy (AOSLO)[16,17] or transscleral optical phase imaging (TOPI),[18] cell shape descriptors and AF measures that reliably characterize individual AMD-affected RPE cells are of particular importance.

We, therefore, quantified RPE morphology using cell shape descriptors and corresponding cellular AF levels in human donor RPE flatmounts with unaffected macula and AMD. We compared the effect of age and topography to that of disease. The results of this study will provide a strong foundation for clinical analysis of RPE cell shape and AF with the ability to identify robust biomarkers for the early detection of diseased AMD cells.

Methods

All protocols were in accordance with the Declaration of Helsinki, and the use of human tissue was approved by the institutional review boards of the

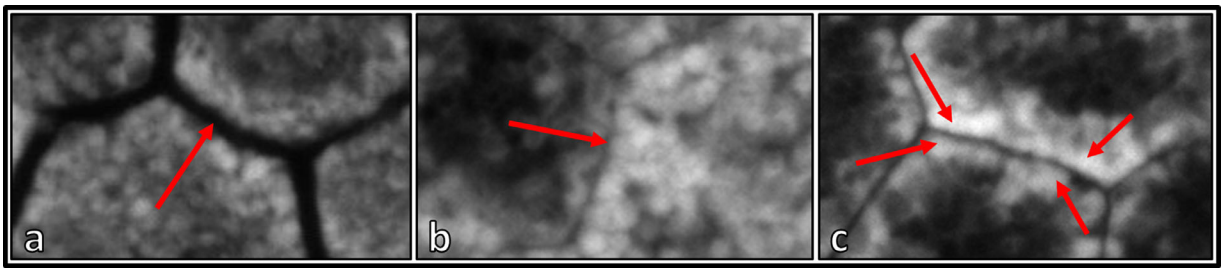

Figure 1. Cell border marking process based on autofluorescent properties. (a) The hypofluorescent/nonfluorescent gap between individual RPE cells. (b) Differences in AF levels between neighboring RPE cells. Autofluorescence of RPE cells in a single slab can be misjudged or altered by the nucleus. It is, therefore, advisable for graders to scroll through the image in the z-direction for labeling. (c) A change in orientation of granules with densely packed granules at the cell border that oftentimes share the same orientation. The granules line up along the plasma membrane, and the lines change direction sharply at a vertex, which then can be marked. All these features were utilized to delineate neighboring RPE cells.

University of Alabama at Birmingham and the University of Bonn, Germany (# 386/20).

Tissues

Seven AMD-affected human RPE flatmounts (4 female/3 male donor eyes; mean age 85 ± 3 years; AMD stages: early, 3; geographic atrophy, 1; neovascular, 3) and 15 human RPE flatmounts from healthy donors (≤51 years, $n = 8$; >80 years, $n = 7$) were used for imaging. Tissue collection, classification, and preparation have been described previously.[6] Briefly, globes were collected from the Advancing Sight Network (Birmingham, AL, USA) within 4.2 hours of death and subsequently prepared and preserved by immersion in 4% paraformaldehyde/0.1 M phosphate-buffered saline (PBS). RPE flatmounts were prepared with removal of the choroid and neuroretina documented by sequential photography to preserve the position of the foveal pit, as illustrated in Supplementary Figure S1 in Ach et al.[1] RPE flatmounts were imaged at three canonical locations: fovea, perifovea (4 mm superior to the fovea), and near periphery at the superior edge of the RPE flatmount (mean distance from the foveal center, 7.45 ± 1.0 mm).[19]

Imaging

RPE flatmounts were imaged using a Zeiss LSM 780 laser-scanning confocal fluorescence microscope (Carl Zeiss Microscopy, Jena, Germany) with an excitation wavelength set at 488 nm and AF emission recorded from 490 to 695 nm in 24 channels (8.9-nm spectral channel width). The scanning area covered 224.92 × 224.92 μm^2, and RPE cells were imaged from the apical RPE (first autofluorescent granules in focus) to basal RPE (last autofluorescent granules out of focus), with a 390-nm step size.

Using FIJI (ImageJ; National Institutes of Health, Bethesda, MD, USA), RPE cells were then manually traced using the polygon selection tool in FIJI to record the X/Y coordinates of vertices.[20] RPE cell borders were estimated by the hypofluorescent gap between two RPE cells, making it possible to mark vertices of presumed plasma membranes, changes in granule orientation (palisade-like orientation of granules at the cell border with a change in direction sharply at a vertex, which then can be marked), or sudden changes in AF intensity (Fig. 1). Only cells in which cell borders could be clearly discriminated were marked and included in subsequent analysis, resulting in a lower RPE cell count and a possible floor effect in AMD (due to exclusion of cells with no delineable borders). The maximum RPE cell count per eye and location was arbitrarily set to 100.

Cell Shape Descriptors

Cell shape descriptors were computed based on the solid shape bounded by the polygon using customized software (available at https://uab.box.com/s/pqtak77d0esfnjkjtv8320s3617k0bxq). Analysis included form factor (= cell perimeter/($4\pi \times$ "*cell area*")), roundness, major and minor axes of the best-fitting ellipse, aspect ratio, compactness, eccentricity, area and perimeter of the convex hull, and centroid.[21] Shape descriptors are further elucidated in Table 1. Cells were expected to be enlarged with age and disease.[22,23] Thus, cell size was assessed with shape descriptors of area, perimeter, and area/perimeter of the convex hull.

Table 1. Shape Descriptors

Shape Descriptor	Explanation
Form factor	Measure for the circularity of a polygon. 4π times the area of the polygon divided by the square of the perimeter.
Roundness	Area of the polygon divided by area of the best-fitting circle.
Major and minor axes of the best-fitted ellipse	Axis of an ellipse, which has the same area as the cell shape. Major: vector from one end of the ellipse to the other end. Minor: vector from one side of the ellipse to the other side.
Aspect ratio	Length divided by breadth of axis-aligned bounding box.
Convex hull	Smallest convex shape, which contains the original shape.
Solidity	Area of the polygon divided by the area of the convex hull.
Convexity	Ratio of perimeter of the convex hull to that of the polygon.
Eccentricity	Ratio of length of major axis to minor axis.
Area	Area of the polygon computed from the vertices.
Perimeter	Distance around the polygon.
Centroid	X-coordinate and y-coordinate of the centroid computed from the polygon.

Autofluorescence Per Cell

Total AF per cell was calculated in a two-step process. First, intensities from all pixels of all slabs in the z-direction and all spectral channels were added in a one-sum-projected image. Following, the intensities of all pixels within this image were summated, resulting in the total AF intensity of the sum-projected cell. Using the same manual markings to extract shape descriptors, the integrated AF intensity of RPE cells was calculated and used for analysis.

In contrast to our previous work where RPE cells were subjectively clustered into six different morphologic phenotypes based on AF and cytoskeleton,[24] the goal of our current work is identifying shape descriptors associated with AF levels that could be used for automated analysis in the future.

Statistical Analysis

For an initial exploratory analysis, we performed a principal component analysis (PCA) on RPE cells for which shape features were available, using z-normalization to avoid distortions due to the different scales of the features.

To investigate the information content of the features, we performed a supervised learning problem using the cell shape descriptors. Due to the structure of the data, where data on a varying number of cells per donor and localization were available, we chose an ensemble classification approach with logistic regression at its core.

For the inference of a "batch" of cells (usually all cells from a certain location in one tissue), each is assigned a label individually by the classifier, and the predicted class label of the whole batch is determined as the most common label of its constituent cells (i.e., by "majority vote").

We utilized the implementation of logistic regression provided by the scikit-learn package for Python. To improve robustness, we chose elastic net regularization with equal weight given to the L^1 and L^2 norms; for this reason, the data were z-normalized for the logistic regression as well.

Evaluation was done by fivefold stratified cross-validation. Additionally, a permutation test for the null hypothesis ("the classifier was not able to find a connection between cell shape descriptors and the donor classes") was performed, where the fitting and evaluation procedure was repeated 1000 times with random labels instead of the true ones. For each run, this yielded an empirical P value calculated as

$$P_{\text{emp}} = \frac{1 + \#\{\text{random label permutations with accuracy at least as good as real labels}\}}{1 + \#\{\text{permutations}\}}$$

This analysis was performed for several independent avenues of investigation: to distinguish (1) between samples taken from patients with AMD and the healthy controls, (2) whether classification is possible between the locations (either using an all-versus-rest approach or between pairs of locations) from only the healthy samples, and (3) whether, among the healthy samples, a differentiation between young and aged donor is possible. For the evaluation of possible differences between locations, two-tailed t-tests were used. We report the empirical P value, which gives an approximation of the

probability to obtain the same accuracy as our classifier or better exclusively by chance (in layman's terms, a classifier is made to simply guess 1000 times, as input data are scrambled randomly, and the odds of guessing better than the actual classification accuracy are reported). *P* values ≤0.05 were regarded as statistically significant.

Finally, to investigate the link between shape and measured AF, we used a linear mixed-effect model (as implemented by the statsmodels package for Python).[25] In this model, each flatmount was considered one group to account for differences in illumination settings between donors. RPE cells from healthy donors were used for this analysis.

Results

From RPE flatmounts of 15 donor eyes with unremarkable maculas, 4278 RPE cells at the three defined locations were included (≤51 years: 726 fovea, 785 perifovea, 741 near periphery; >80 years: 626 fovea, 700 perifovea, 700 near periphery). From seven AMD-affected RPE flatmounts, a total of 1108 RPE cells at the three locations (75 fovea, 427 perifovea, 606 near periphery) were included (Fig. 2).

Age-Related Differences of RPE Morphology

In donors with unaffected macula, cell shape descriptors between young and aged donors were not significantly different (empirical *P* values: fovea = 0.5; perifovea = 0.49; near periphery = 0.65; Fig. 2). Uniformly at all locations, however, a trend toward increased area and reduced form factor with age can be observed.

AMD-Dependent Changes in RPE Morphology

Our first line of inquiry was to distinguish between healthy and AMD donors based on the extracted cell shape descriptors (Fig. 3). The results of the ensemble logistic regression classification are summarized in Table 2.

Clear morphologic changes between healthy and AMD samples at all three locations are determinable (Fig. 4). Notably, the classification based exclusively on foveal cells was able to achieve perfect accuracy on all training and test samples of each fold. For the other locations, the differences are not as pronounced, but a genuine structure of the data is nonetheless clearly recovered by the logistic regression (Fig. 5). The sets of parameters estimated for each training fold are shown in Figure 5 and demonstrate that in

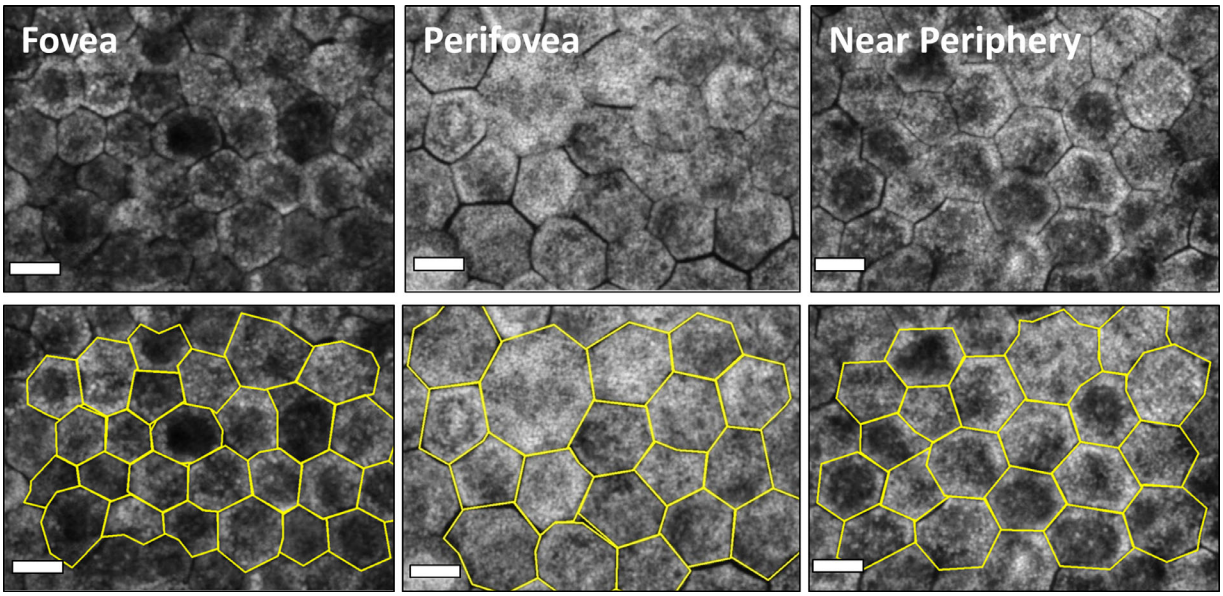

Figure 2. RPE cell monolayer at three locations (fovea, perifovea, near periphery) of healthy donors with and without marked cell borders. RPE flatmounts imaged with a confocal fluorescence microscope (excitation: 488 nm) at three predefined locations. The tissues are from healthy donors: 81 years, 85 years, and 83 years old, respectively (from *left* to *right*). *Bottom row*: the RPE cell borders are delineated in *yellow*. The image clearly demonstrates the RPE cell size differences between the fovea and extrafoveal locations. Also, due to high lipofuscin granule load, perifoveal RPE cells appear to have the highest autofluorescence signal compared to foveal and near-peripheral RPE cells. *Scale bar*: 10 µm.

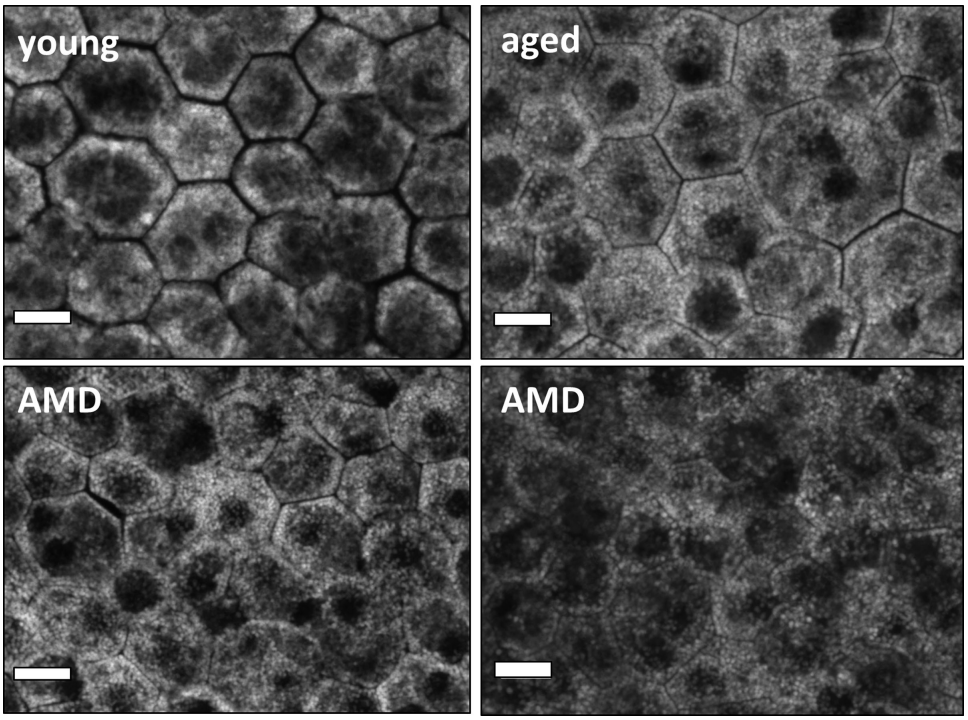

Figure 3. RPE morphology in normal and AMD-affected donors. RPE cells from four different donors imaged at the perifovea using 488-nm excitation and capturing the autofluorescence emission signal. *Top row*: representatives of the unaffected perifovea from a healthy young (36 years) and healthy aged (90 years) donor. In both, the polygonal patterns can be identified. Healthy young RPE cells tend to be smaller and on visual inspection less autofluorescent. *Bottom row*: the perifovea of two AMD-affected donors (*left*, 86 years; *right*, 84 years). In AMD, RPE cell delineation is difficult and RPE cells tend to be enlarged. *Scale bar*: 10 µm.

Table 2. Results of Logistic Regression for Differences Between Healthy (Young and Aged Pooled) and AMD-Affected RPE Cells

Localization	Average Accuracy in Fivefold Cross-Validation	Empirical *P* Value
All cells pooled	0.95	<0.001
Fovea	1.00	<0.001
Perifovea	0.83	0.015
Near periphery	0.77	0.036

particular, an increase in area was a clear indicator for AMD, at all locations. For the perifovea and near periphery, AMD was also associated with a lower form factor (shape descriptor; round shapes are high in form factor). Additionally, at the near periphery, increased convexity and decreased solidity (shape descriptor; shapes with spurs are low in solidity) were estimated to be indicative of AMD. Since the fitting process of the logistic regression included a regularization term, no explicit construction of confidence intervals on the parameters is possible. However, it is clear from the magnitude of the coefficients (roundness, form factor, convexity, solidity, area) that both for perifovea and near periphery, there is a significantly higher degree of uncertainty (also reflected in the classification performance). We further analyzed changes between healthy and early AMD samples at all three locations, which demonstrated similar estimated values as the "all" AMD/healthy model. Likely due to the low sample size of AMD RPE cells, only differences in fovea proved statistically significant (fovea, 1/0.001 [accuracy/empirical *P* value]; perifovea, 0.88/0.06; near periphery, 0.8/0.1). Similarly, in a set of only healthy-aged/AMD model, almost identical estimated values were computed, but only the fovea proved statistically significant (fovea, 1/0.003 [accuracy/empirical *P* value]; perifovea, 0.73/0.11; near periphery, 0.63/0.23).

Topographic Variances in RPE Morphology

Differentiating between the locations based on data from the healthy donors presents a ternary instead of a binary classification problem (see Fig. 2). Thus, we chose a one-versus-rest scheme, estimating three separate sets of coefficients, each representing association of the features with a given location. Additionally, we considered the three possible juxtapositions of

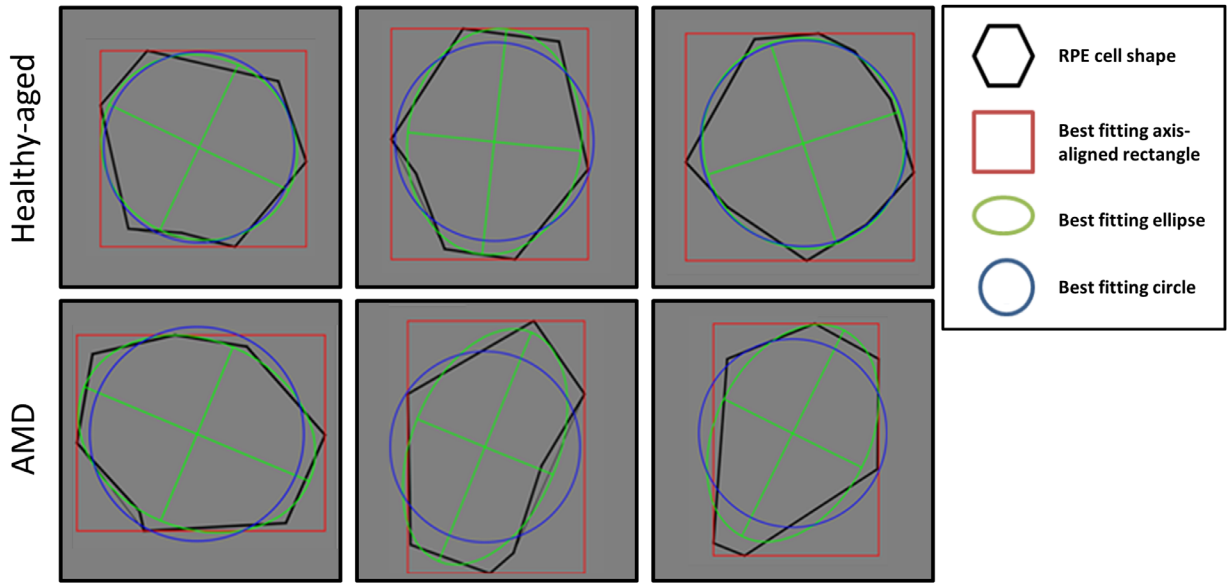

Figure 4. Cell shape descriptors. Shape descriptors of six exemplary perifoveal RPE cells from two donors (AMD [84 years old] and unremarkable macula [90 years old]). The *black shapes* contour the outline of the RPE cells. In *green*, *blue*, and *red* are the best-fitting ellipse, circle, and square, respectively. Healthy-aged RPE cells are almost uniformly hexagonal. In AMD, RPE cells seem elongated and dysmorphic. Shape descriptors of RPE cells in AMD show lower values in solidity, roundness, and form factor, all associated with AMD.

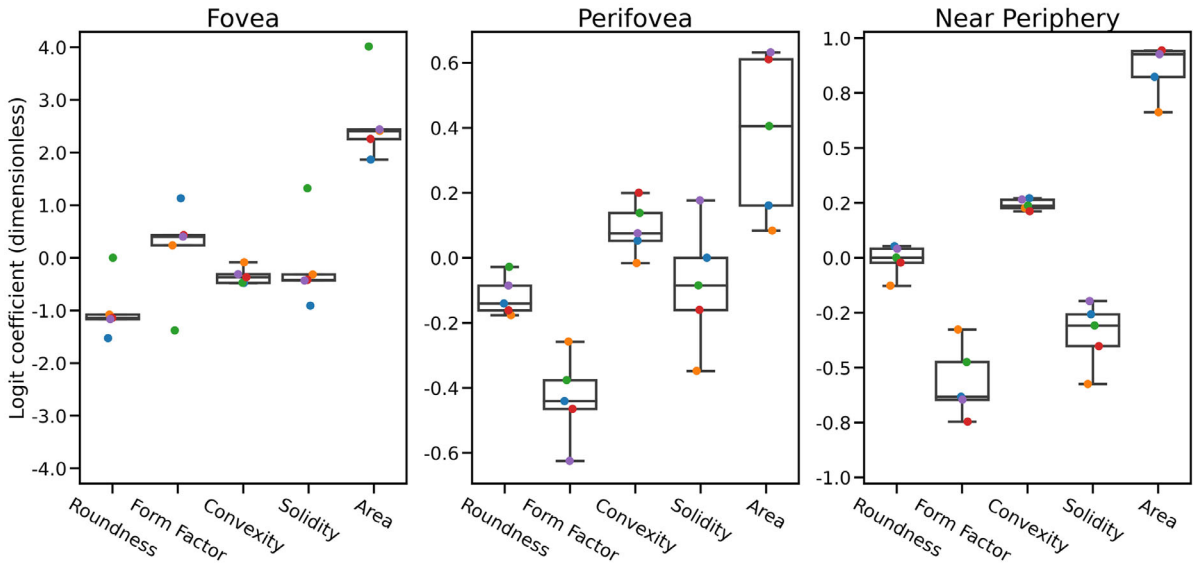

Figure 5. Estimated parameters for "AMD vs. healthy" models. Parameters estimated by logistic regression: each *color-coded dot* corresponds to one round of cross-validation. From *bottom* to *top*, the boxplots show minimum, first quartile, median, third quartile, and maximum. The y-axis is aligned at zero but scaled differently due to large variability in effect size. High positive values on the y-axis indicate correlation with the presence of AMD, and high negative values indicate anticorrelation. Increased cell size (area) seems to be a location-independent indicator of AMD, potentially together with decreased roundness. Furthermore, reduced form factor and solidity are indicative for the presence of AMD outside of the fovea.

locations, which again are binary classifications. The results are summarized in Table 3, and the parameters are given in Figure 6. While classification in this case is far from perfect with an average validation accuracy of 0.59, the permutation test ($P < 0.001$) reveals that it is much better than a "guessing" classifier could be expected to be. The perifovea forms a kind of middle ground between fovea and near periphery, as the binary classification between these two extreme cases yields the best results. Overall, closeness to the

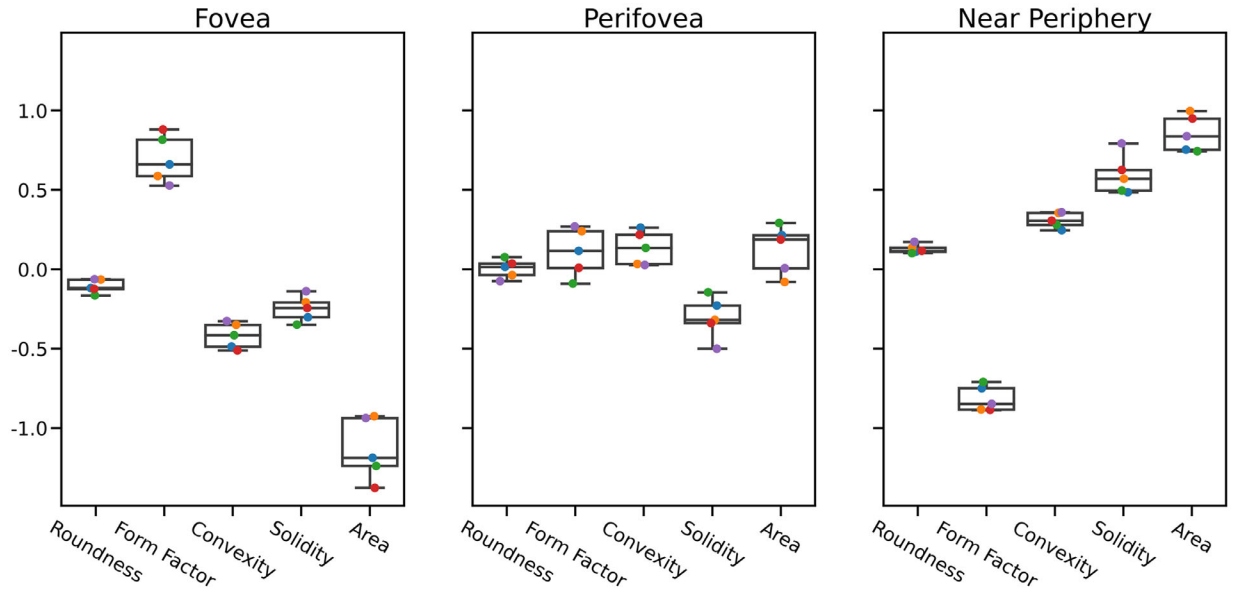

Figure 6. Estimated parameters for location-specific differences: "one-versus-rest" models. Parameters estimated by logistic regression. Each *color-coded dot* corresponds to one round of cross-validation. From *bottom* to *top*, the boxplots show minimum, first quartile, median, third quartile, and maximum. Large positive values on the y-axis indicate correlation with the given tissue, and large negative values indicate anticorrelation. Estimated parameters for location-specific RPE morphology alterations (classification of each location versus the rest). Area and form factor seem to delineate foveal and near-peripheral cells quite well. Perifoveal cells appear to be in the middle, so a subsequent comparison to individual locations was performed (see Results section).

Table 3. Results of Logistic Regression for Topographic Differences of RPE Cells

Setting	Average Accuracy in Fivefold Cross-Validation	Empirical *P* Value
One-versus-rest	0.59	<0.001
Fovea vs. perifovea	0.73	0.01
Fovea vs. near periphery	0.90	<0.001
Perifovea vs. near periphery	0.56	0.289

fovea is strongly linked with higher form factor and lower area, as well as associated with lower convexity and solidity.

RPE Morphology and AF

Lower roundness and solidity were associated with significantly higher AF ($P = 0.003$ and $P = 0.015$, respectively) (Table 4). None of the other features had a statistically significant correlation, although the data show a trend of higher AF to be correlated with higher form factor as well as larger cell area ($P = 0.089$ and $P = 0.057$, respectively).

Discussion

In this study, we applied cell shape analysis to assess differences in RPE morphology with age, location, and AF intensity in both healthy and AMD-affected human donor eyes. Our main findings were that RPE cells enlarge and display dysmorphia with age, increasing eccentricity from the fovea, and with the presence of AMD. This work highlights the potential of using RPE morphology and AF alterations for the early detection of AMD disease onset.

We consider our computational approach of cell descriptors to benefit the accuracy of cell shape description with possible future applications. The shape descriptors presented here, based on the solid shape bounded by the polygon, provide three key advantages. Shape descriptors are (1) an objective measurement of cell shape, which facilitates future automated image analysis approaches and could be applied to evaluate cultured RPE cells with big sample sizes. Moreover, (2) not relying on pixel-based analysis allows extrapolating this approach more easily to

Table 4. Results of Linear Mixed Model for the Association of Autofluorescence With Shape Descriptors in RPE Cells of Donors Without AMD

Characteristic	Coefficient	Standard Error	*Z* Value	$P > \|z\|$	Confidence Interval (0.025 to 0.0975)
Intercept	−0.004	0.136	−0.033	0.974	−0.272 to 0.263
Roundness	−0.025	0.008	−2.998	0.003	−0.042 to −0.009
Form factor	0.023	0.014	1.699	0.089	−0.004 to 0.050
Convexity	0.011	0.011	1.019	0.308	−0.011 to 0.033
Solidity	−0.030	0.012	−2.426	0.015	−0.054 to −0.006
Area	0.017	0.009	1.902	0.057	−0.001 to 0.035

Column headings: Coefficient = β-coefficient for this effect of the model; standard error = standard deviation of this coefficient; *Z* value = the coefficient divided by the standard error; $P > |z|$ = standard deviation of the coefficient point estimate; confidence interval = upper and lower limits of the 95% confidence interval of the coefficient. Row headings: shape descriptors used in the linear mixed model (and intercept). Shape descriptors with strong correlation among each other were excluded from analyses.

other images with different resolution and enables different approaches of contour detection. Finally (3), using both size-dependent and size-independent shape descriptors may more comprehensively describe RPE cell dysmorphia in AMD (i.e., beyond cell enlargement).

Our data indicate that the RPE cell shape descriptors remain rather stable in normal aging with a trend of cell enlargement and some loss of form factor. The cytoskeleton of the RPE is responsible for maintaining the shape of the cell, spatially organizing granules, mitochondria, and nucleus within the cell and interacting with its environment outside the cell.[26] The RPE cytoskeleton mainly consists of actin, microtubules, and intermediate filaments.[2,27] In combination with a multitude of cytoplasmic proteins, the latter form an adaptive structure capable of constant remodeling.[28] One reason for this great stability of the RPE cell shape could be the Wnt/β-catenin pathway and its role on the cadherin-based cell–cell adhesion.[29] This complex pathway regulates cadherin binding and protects the RPE from oxidative stress.[30] Dysregulation of the WNT/β-catenin pathway could also explain differences in RPE cell shape alterations with age. If β-catenin is downregulated, oxidative modification of cytoskeletal proteins can occur, ultimately leading to RPE shape variations. Age-related sublethal oxidative stress is a possible driver of RPE dysmorphia, supported by smoking as an oxidative stressor leading to an altered RPE monolayer.[31] Further, chronic inflammation could contribute to the initiation and progression of shape alterations and serve as an oxidative stressor. At this point, it is unclear whether these alterations are important to monitor or if they remain without consequence. An altered RPE monolayer, however, may not be able to maintain outer retinal health and properly serve the overlying photoreceptors, as intended. Because differences in cell shape may not affect all cells and locations but nonetheless have strong implications for a functioning retina, cell shape descriptors could serve to characterize these alterations in more detail. Therefore, information extracted from cell shape alterations in aging could even have clinical utility in the future. First, being able to distinguish young from aged and healthy from disease-affected RPE cells may help to better examine the effect of different agents in vitro (oxidative stress, chemical oxidants, or light irradiation).[32] Second, structure–function correlations could help answer whether subcellular RPE alterations as seen in normal aging have potential functional implications.[23] Last, cell shape analysis could serve to evaluate RPE transplants and/or future organoids prior to the in vivo insertion of tissue.[33–35]

We were able to identify topographical differences throughout the RPE cell monolayer in healthy donors. Local differences between the fovea and the perifovea may stem from different functional requirements and a changing compilation of the human photoreceptor mosaic imbedded into the microvilli of RPE cells.[3] The cone photoreceptor density peaks at the foveal center and decreases 10-fold at 3.5° (1 mm) eccentricity. This makes the analysis of RPE cells in relation to the foveal center important. In this study, RPE cell location–specific analysis was achieved through serial photography.[1] Furthermore, the specific photoreceptor topography and adapted RPE sheet also make the use of human tissue instead of animal tissue a requirement to analyze the RPE as part of the visual axis.[5,36]

How postmitotic RPE achieves and maintains its cell formation is also of great interest for research on stem cell–derived RPE cells for human implants. An intact cell formation is necessary to ensure the RPE's barrier function and polarized secretion of growth factors.[34] As mentioned, to date, a gross visual inspection of the RPE´s polygonal appearance is used to define the phenotype and cell differentiation of RPE stem cells.[37] Our analysis proposed here could fill the unmet need of more accurately analyzing cell shape and comparing it with the histologic location it is designed to mimic. This could allow fabricating an RPE sheet that is adapted to its location-specific requirements and optimally serving the photoreceptor mosaic as intended.

Apart from the variance in unaffected RPE cells, the major focus of this study was to identify RPE cell dysmorphia within the AMD-affected macula. We noticed that RPE cell shape was altered in most but not all RPE cells in AMD-affected tissues and differed strongly between individuals and especially locations. These local differences could be a response to different disease processes restricting the RPE predominantly in the central macula. Extracellular deposits (e.g., drusen, basal linear deposits, basal laminar deposits [BLamD], subretinal drusenoid deposits [SDDs]) can lead to an impaired transport between RPE and its adjacent tissue and be a trigger of cell shape alterations. Foveal RPE cells are most frequently exposed to sub-RPE drusen-related RPE detachments and macular neovascularization as well as age- and disease-related progressive insertion of BLamD.[38]

Despite the differences in the fovea, the computational approach was demonstrated to identify cell shape differences in the perifovea and near periphery as well and thus could serve in detecting earliest differences and may even predict the onset of lesions. Albeit sub-RPE drusen are scarce in the perifovea, other lesions (e.g., hard drusen, cuticular drusen, SDDs) could have a similar effect on RPE cell dysmorphia.[39] In the near periphery, the impact of drusen-related material may be negligible, and the risk of these lesions is assumed to be confined to the central macula. Nonetheless, the near periphery may still be affected by an accumulation and expansion of BLamD known to be associated with a high degree of RPE dysmorphia.[40,41]

In light of the here identified RPE area increase in all retinal regions associated with AMD, the question arises if RPE cell loss or cell stacking occurs to cope with these changes. One study found no altered number of total RPE cells associated with AMD in the RPE cells investigated here.[8] An indication that some loss and migration of RPE cells occur is the presence of hyperreflective foci in optical coherence tomography (OCT) imaging, which are believed to be migrating RPE cells.

Our results indicate that RPE shape and AF are intertwined, but the changes in AF do not fully explain the herein described changes in AMD-related RPE cell shape. Higher AF was correlated with decreased solidity and roundness of the RPE, but overall, only a rather small effect could be identified. Further, as RPE cell AF was compared only to cells of the same flatmount and location (as no quantitative approach with a fluorescence probe was used), the results should be interpreted cautiously. A recent histologic study showed that in AMD RPE cells, intracellular organelle distribution (apical: melanosomes/melanolipofuscin; basal/basolateral: lipofuscin dominated) was comparable to aged RPE cells.[42] Further, this study showed that lipofuscin and melanolipofuscin, the predominant source of short-wavelength AF of the human RPE, were reduced in AMD RPE cells.[42] Histologic studies have documented RPE degranulation, shedding, and anterior migration to be at least partly culpable for the reduced AF of the monolayer.[1] Further, there is an increasing amount of evidence that AMD is associated with decreased rather than increased autofluorescence in clinical imaging.[10] Also, as shown in experimental models, photo-oxidation and photolysis are possible mechanisms that might lead to altered lipofuscin bisretinoids and, consequently, can result in a decrease in AF.[43] The comparison between RPE cell shape and quantified AF between donors with and without AMD is therefore a focus of our future studies. Additionally, autofluorescence spectra (e.g., blue-shifted spectral curves in AMD) in combination with cell shape descriptors may help delineate diseased RPE cells more accurately in the future.[44]

Strengths of this study include the use of multiple tissues from different age groups and a clear distinction between affected and unaffected macula, well-preserved RPE flatmounts with short postmortem time, the use of human tissue, and a high number of manually marked RPE cells from precisely defined locations with the exact position of the fovea as its center.[1,6] Our study should also be examined in light of its weaknesses. RPE cells were marked without staining the RPE F-actin cytoskeleton (e.g., with phalloidin) but rather by using confocal microscopy for AF only. While this method may handicap accurate delineation in some cases, it is compatible with in vivo adaptive optics–assisted imaging and may ease automated segmentation and structure–structure correlation of these two modalities in the future.[16] Further refraining from using additional markers made delineation less reliable but also made it possible to measure AF without

obstruction from fluorescence of the markers and to correlate AF with shape descriptors. Another weakness is the limited number of RPE cells in the AMD-affected fovea. Further, our use of RPE flatmounts hindered analysis of anteriorly migrating RPE cells seen as hyperreflective foci in OCT imaging. For this purpose, additional cross-sectional studies of the RPE with the neuroretina attached would have been preferable. Further, due to the use of RPE flatmounts, it cannot be excluded that BLamD or basal linear deposits (BLinD) might be responsible for detected shape descriptor alterations in this study. However, in all areas analyzed, drusen breaking through the RPE monolayer and heavily affecting cell shape were not visible. Future studies, combining en face and cross-section microscopy, could address this in more detail. Future studies should focus on early AMD manifestations to accurately quantify RPE dysmorphia prior to atrophy and/or macular neovascularization. Further, the parafovea would be well suited for these analyses, as it has shown to be critical in the onset of AMD.

In summary, this study demonstrates RPE cell shape alterations dependent on age, location within the retina, autofluorescence, and the presence of AMD. The morphology analysis presented here should be seen as a steppingstone for future fully automated analysis of cell shape features (e.g., in human stem cell–derived RPE implants and AOSLO or TOPI in healthy and AMD-affected subjects).

Acknowledgments

Supported by NIH/NEI 1R01EY027948-01 (TA, CAC), R01EY029595 (CAC), and R01EY024378 (CAC); the German Research Foundation under Germany's Excellence Strategy EXC 2047/1–390685813 and EXC 2151–390873048; and Gerok Research Grant (BONFOR O-137.0030, Faculty of Medicine, University of Bonn, Bonn, Germany) (MS). Tissues were provided by NIH R01EY06109 (CAC).

Disclosure: **L. von der Emde**, None; **M. Vaisband**, None; **J. Hasenauer**, None; **L. Bourauel**, None; **K. Bermond**, None; **M. Saßmannshausen**, Carl Zeiss MedicTec AG (F), CenterVue (F), Heidelberg Engineering (F); **R. Heintzmann**, Carl Zeiss (F, C); **F.G. Holz**, Acucela (C, F), Allergan (F), Apellis (C, F), Bayer (C, F), Boehringer-Ingelheim (C), Bioeq/Formycon (F, C), CenterVue (F), Ellex (F), Roche/Genentech (C, F), Geuder (C, F), Graybug (C), Gyroscope (C), Heidelberg Engineering (C, F), IvericBio (C, F), Kanghong (C, F), LinBioscience (C), NightStarX (F), Novartis (C, F), Optos (F), Oxurion (C), Pixium Vision (C, F), Stealth BioTherapeutics (C), Zeiss (F, C); **C.A. Curcio**, Genentech (F), Regeneron (F), Heidelberg Engineering (F); **K.R. Sloan**, None; **T. Ach**, Roche (C), Novartis (C), Novartis (R), Bayer (C), Apellis Pharmaceuticals (C)

References

1. Ach T, Huisingh C, McGwin G, et al. Quantitative autofluorescence and cell density maps of the human retinal pigment epithelium. *Invest Ophthalmol Vis Sci*. 2014;55:4832–4841.
2. Tarau I-S, Berlin A, Curcio CA, Ach T. The cytoskeleton of the retinal pigment epithelium: from normal aging to age-related macular degeneration. *Int J Mol Sci*. 2019;20:3578.
3. Curcio CA, Millican CL, Allen KA, Kalina RE. Aging of the human photoreceptor mosaic: evidence for selective vulnerability of rods in central retina. *Invest Ophthalmol Vis Sci*. 1993;34:3278–3296.
4. Chen M, Rajapakse D, Fraczek M, Luo C, Forrester JV, Xu H. Retinal pigment epithelial cell multinucleation in the aging eye—a mechanism to repair damage and maintain homoeostasis. *Aging Cell*. 2016;15:436–445.
5. Rashid A, Bhatia SK, Mazzitello KI, et al. RPE cell and sheet properties in normal and diseased eyes. *Adv Exp Med Biol*. 2016;854:757–763.
6. Bermond K, Wobbe C, Tarau IS, et al. Autofluorescent granules of the human retinal pigment epithelium: phenotypes, intracellular distribution, and age-related topography. *Invest Ophthalmol Vis Sci*. 2020;61:35.
7. Pröbster C, Tarau IS, Berlin A, et al. Quantitative fundus autofluorescence in the developing and maturing healthy eye. *Transl Vis Sci Technol*. 2021;10:15.
8. Ach T, Tolstik E, Messinger JD, Zarubina AV, Heintzmann R, Curcio CA. Lipofuscin redistribution and loss accompanied by cytoskeletal stress in retinal pigment epithelium of eyes with age-related macular degeneration. *Invest Ophthalmol Vis Sci*. 2015;56:3242–3252.
9. Reiter GS, Told R, Schlanitz FG, et al. Impact of drusen volume on quantitative fundus autofluorescence in early and intermediate age-related macular degeneration. *Invest Ophthalmol Vis Sci*. 2019;60:1937–1942.
10. von der Emde L, Guymer RH, Pfau M, et al. Natural history of quantitative autofluorescence

in intermediate age-related macular degeneration. *Retina*. 2021;41(4):694–700.
11. Liu Z, Kocaoglu OP, Miller DT. 3D imaging of retinal pigment epithelial cells in the living human retina. *Invest Ophthalmol Vis Sci*. 2016;57:OCT533–OCT543.
12. Pfau M, Lindner M, Goerdt L, et al. Prognostic value of shape-descriptive factors for the progression of geographic atrophy secondary to age-related macular degeneration. *Retina*. 2019;39:1527–1540.
13. Kocher AA, Schuster MD, Szabolcs MJ, et al. Neovascularization of ischemic myocardium by human bone-marrow-derived angioblasts prevents cardiomyocyte apoptosis, reduces remodeling and improves cardiac function. *Nat Med*. 2001;7:430–436.
14. Chen CS, Mrksich M, Huang S, Whitesides GM, Ingber DE. Geometric control of cell life and death. *Science*. 1997;276:1425–1428.
15. Zdilla MJ, Hatfield SA, McLean KA, Cyrus LM, Laslo JM, Lambert WH. Circularity, solidity, axes of a best fit ellipse, aspect ratio, and roundness of the foramen ovale: a morphometric analysis with neurosurgical considerations. *J Craniofac Surg*. 2016;27:222–228.
16. Granger CE, Yang Q, Hongxin S, et al. Human retinal pigment epithelium: in vivo cell morphometry, multispectral autofluorescence, and relationship to cone mosaic. *Invest Ophthalmol Vis Sci*. 2018;59:5705–5716.
17. Vienola KV, Zhang M, Snyder VC, Sahel J-A, Dansingani KA, Rossi EA. Microstructure of the retinal pigment epithelium near-infrared autofluorescence in healthy young eyes and in patients with AMD. *Sci Rep*. 2020;10:9561.
18. Laforest T, Kü;nzi M, Kowalczuk L, Carpentras D, Behar-Cohen F, Moser C. Transscleral optical phase imaging of the human retina. *Nat Photonics*. 2020;14:439–445.
19. Polyak S. *The Retina: The Anatomy and the Histology of the Retina in Man, Ape, and Monkey, Including the Consideration of Visual Functions, the History of Physiological Optics, and the Histological Laboratory Technique*. Boca Raton, Florida: CRC Press Inc; 1941.
20. Schindelin J, Arganda-carreras I, Frise E, et al. Fiji: an open-source platform for biological-image analysis. *Nat Methods*. 2012;9:676–682.
21. Russ JC. *The Image Processing Handbook*. CRC Press; 2017.
22. Nagai H, Kalnins VI. Normally occurring loss of single cells and repair of resulting defects in retinal pigment epithelium in situ. *Exp Eye Res*. 1996;62:55–61.
23. Jiang Y, Qi X, Chrenek MA, et al. Functional principal component analysis reveals discriminating categories of retinal pigment epithelial morphology in mice. *Invest Ophthalmol Vis Sci*. 2013;54:7274–7283.
24. Gambril JA, Sloan KR, Swain TA, et al. Quantifying retinal pigment epithelium dysmorphia and loss of histologic autofluorescence in age-related macular degeneration. *Invest Ophthalmol Vis Sci*. 2019;60:2481–2493.
25. Seabold S, Perktold J. Statsmodels: Econometric and statistical modeling with python. In van der Walt S, Millman J, eds. *Proceedings of the 9th Python in Science Conference*, 2010:92–96, https://doi.org/10.25080/Majora-92bf1922-011.
26. Fletcher DA, Mullins RD. Cell mechanics and the cytoskeleton. *Nature*. 2010;463:485–492.
27. McKechnie NM, Boulton M, Robey HL, Savage FJ, Grierson I. The cytoskeletal elements of human retinal pigment epithelium: in vitro and in vivo. *J Cell Sci*. 1988;91(pt 2):303–312.
28. dos Remedios CG, Chhabra D, Kekic M, et al. Actin binding proteins: regulation of cytoskeletal microfilaments. *Physiol Rev*. 2003;83:433–473.
29. Nelson WJ, Nusse R. Convergence of Wnt, beta-catenin, and cadherin pathways. *Science*. 2004;303:1483–1487.
30. Gavert N, Ben-Ze'ev A. Beta-catenin signaling in biological control and cancer. *J Cell Biochem*. 2007;102:820–828.
31. Wang AL, Lukas TJ, Yuan M, Du N, Handa JT, Neufeld AH. Changes in retinal pigment epithelium related to cigarette smoke: possible relevance to smoking as a risk factor for age-related macular degeneration. *PLoS One*. 2009;4:e5304.
32. Hayes MJ, Burgoyne T, Wavre-Shapton TS, Tolmachova T, Seabra MC, Futter CE. Remodeling of the basal labyrinth of retinal pigment epithelial cells with osmotic challenge, age, and disease. *Invest Ophthalmol Vis Sci*. 2019;60:2515–2524.
33. Binder S, Stanzel BV, Krebs I, Glittenberg C. Transplantation of the RPE in AMD. *Prog Retin Eye Res*. 2007;26:516–554.
34. Schaub NJ, Hotaling NA, Manescu P, et al. Deep learning predicts function of live retinal pigment epithelium from quantitative microscopy. *J Clin Invest*. 2020;130:1010–1023.
35. Liu S, Xie B, Song X, et al. Self-formation of RPE spheroids facilitates enrichment and expansion of hiPSC-derived RPE generated on retinal

organoid induction platform. *Invest Ophthalmol Vis Sci*. 2018;59:5659–5669.
36. Bhatia SK, Rashid A, Chrenek MA, et al. Analysis of RPE morphometry in human eyes. *Mol Vis*. 2016;22:898–916.
37. Joshi R, Mankowski W, Winter M, et al. Automated measurement of cobblestone morphology for characterizing stem cell derived retinal pigment epithelial cell cultures. *J Ocul Pharmacol Ther*. 2016;32:331–339.
38. Sura AA, Chen L, Messinger JD, et al. Measuring the contributions of basal laminar deposit and bruch's membrane in age-related macular degeneration. *Invest Ophthalmol Vis Sci*. 2020;61:19.
39. Wu Z, Fletcher EL, Kumar H, Greferath U, Guymer RH. Reticular pseudodrusen: a critical phenotype in age-related macular degeneration. *Prog Retin Eye Res*. 2022;88:101017.
40. Marshall J, Hussain AA, Starita C, Moore DJ, Patmore AL. Aging and Bruch's membrane. *Retin Pigment Ep*. New York: Oxford University Press; 1988:669–692.
41. Handa JT, Verzijl N, Aotaki-Keen A, et al. Increase in the advanced glycation end product pentosidine in Bruch's membrane with age. *Invest Ophthalmol Vis Sci*. 1999;40:775–779.
42. Bermond K, von der Emde L, Tarau IS, et al. Autofluorescent organelles within the retinal pigment epithelium in human donor eyes with and without age-related macular degeneration. *Invest Ophthalmol Vis Sci*. 2022;63:23.
43. Kim HJ, Montenegro D, Zhao J, Sparrow JR. Bisretinoids of the retina: photo-oxidation, iron-catalyzed oxidation, and disease consequences. *Antioxidants (Basel, Switzerland)*. 2021;10(9):1382.
44. Bourauel L, Vaisband M, von der Emde L, et al. Spectral analysis of human retinal pigment epithelium cells in healthy and AMD affected eyes. *Invest Ophthalmol Vis Sci*. 2022;63:4621–F0413.